ISSN 1809-5860

COHESIVE CRACK APPROACH TO DEBONDING ANALYSIS

Giuseppe Cocchetti[1], Claudia Comi[2], Umberto Perego[3]

Abstract

Debonding of coatings from substrate due to coating compression occurs in many engineering applications. A simplified analytical approach for the estimation of the ultimate coating compression leading to debonding is developed in this paper, assuming an assigned out-of-plane defect of the coating. The formulation is based on the solution of a beam on a Pasternak (two parameters) elastic foundation, and on the assumption of a Mode I cohesive failure of the coating-substrate interface. The resulting formulas are simple and require the knowledge of a limited number of parameters.

Keywords: Adhesive Joints. Cohesive Model. Coating. Pasternak Foundation.

1 INTRODUCTION

The estimate of the limit capacity of adhesive lap joints is an important engineering problem, since the majority of structural failures are reported to take place starting from joints, and it has attracted the attention of many researchers over the years and given rise to a number of different approaches. A particular type of joint, constituted by an eccentrically compressed layer of coating attached onto a substrate by an adhesive, is considered in this paper (see Figure 1). An interesting example of these type of coatings is represented by civil tile claddings, usually employed for both floorings and external walls of civil buildings, where the eccentricity is the consequence of out-of-plane defects due to poor workmanship in tile placement.

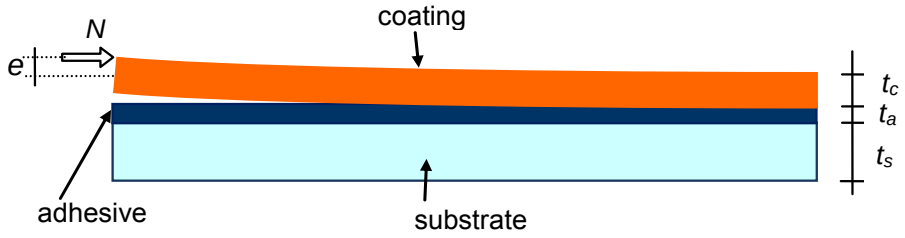

Figure 1 – Scheme of the problem.

Strength based approaches to the failure of joints were initiated by the early works of Volkersen (1938) and Goland and Reissner (1944) for single lap joints, where perfect elasticity of both adhesive and adherends was postulated, and have undergone a continuous refinement over the years (see e.g. Bigwood and Crocombe, 1989; Tsai et al., 1998; Tong, 1998; Yang et al., 2004). Fracture mechanics approaches for a plate debonding from a rigid substrate, have been studied by several authors, in particular for the analytical modeling of the peel test. Among others, De Lorenzis and Zavarise (2008) used the estimates of the energy released during peeling provided by Williams (1997) and Thouless

[1] Department of Structural Engineering, Politecnico di Milano, Italy, giuseppe.cocchetti@polimi.it
[2] Department of Structural Engineering, Politecnico di Milano, Italy, claudia.comi@polimi.it
[3] Department of Structural Engineering, Politecnico di Milano, Italy, umberto.perego@polimi.it

and Jensen (1992) to obtain an analytical mixed mode prediction of fracture propagation conditions to be compared with finite element simulations. Yuan et al. (2007) studied the elastic response of a thin plate bonded to a rigid substrate under peeling load as a beam on a Pasternak foundation (Pasternak, 1954), though without providing a complete explicit analytical solution. The Mode I closed form solution discussed by Williams and Hadavinia (2002) appears to be particularly useful for the purposes pursued in the present paper and will be used as a starting point for the developments required for the study of the problem in Figure 1.

In recent years, the problem of the debonding of different lap joint configurations has also been the object of numerical finite element simulations by several authors. See e.g. Andruet et al. (2001), Gonçalves et al. (2002), Schmidt and Edlund (2006), Edlund et al. (2009), Gustafson and Waas (2009) and Mahaboonpachai et al. (2010). Venturini and coworkers, developed boundary element approaches for cohesive crack structural analyses (see e.g. Manzoli and Venturini, 2007, Leonel and Venturini, 2009 and 2010, Ferreira et al. 2011).

In the proposed simplified approach, it is assumed that debonding occurs according to a Mode I mechanism, described through a cohesive interface between the coating and a rigid support. In the considered problem, the compression force N has an eccentricity e and generates a bending moment Ne at the coating edge which acts as driving force for decohesion. Two different assumptions have been considered for the behavior of the adhesive interface: a linear elastic behavior up to failure or a rigid-cohesive behavior as shown in Figure 3. In both cases, it is possible to compute the limit state in closed form (Williams and Hadavinia, 2002, Carpinteri et al., 2008) and hence determine a bilateral bound for the safety margin of the adopted coating. Reference is made to the geometry and material properties of a specific, realistic joint configuration, corresponding to a tile of a civil flooring placed onto a concrete substrate.

The following notation will be used for each material i: E_i = Young's modulus, ν_i = Poisson's ratio, G_i = shear modulus, $E_i^* = \dfrac{E_i}{1-\nu_i^2}$ = plane strain modulus, t_i = thickness, with $i = c, a, s$ for coating, adhesive and substrate, respectively. Small strains and displacements and negligible second order effects are assumed throughout the paper.

2 ELASTIC DEBONDING LIMIT

The problem considered in the present work is shown in Figure 1: it concerns the possible debonding of a coating joined to a substrate by an adhesive layer. Debonding is assumed to be caused by an eccentric compression force N which produces the bending moment Ne at the coating edge. The limit value of N in the coating, which triggers the decohesion mechanism, can be computed in closed form using the simplified model proposed by Williams and Hadavinia (2002). The coating is modeled as an elastic Euler-Bernoulli beam of length L laying on an elastic-fracturing spring bed constituted by the adhesive (see Figure 2). To determine the elastic limit of the system, the adhesive is modeled as an elastic-brittle interface (model (a) in Figure 3), while to determine the ultimate strength, the adhesive is modeled as a rigid-cohesive interface (model (b) in Figure 3). The free body diagrams of a coating element is shown in Figure 2 for the Pasternak type assumption (two elastic parameters) on the adhesive behavior which will be considered in what follows; the simpler Winkler type model (one elastic parameter) is recovered as a special case for vanishing shear stiffness k_2.

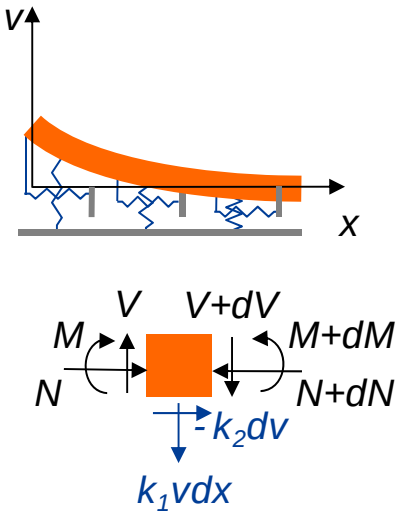

Figure 2 – Coating on spring bed, Pasternak model.

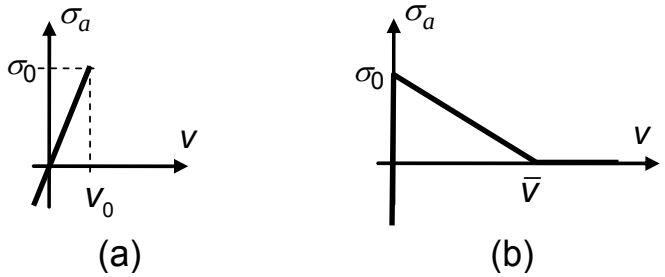

Figure 3 – Constitutive behavior of the adhesive: (a) elastic model (b) rigid-cohesive model.

For the elastic-brittle interface, considering the Pasternak idealization of the adhesive with spring constant $k_1 = E_a^* / t_a$ and $k_2 = \dfrac{G_a\, t_c}{2t_a}$, the transversal displacement v is obtained from the following differential equation

$$\frac{d^4v}{dx^4} - \frac{t_c^2 G_a}{4t_a E_c^* I_c}\frac{d^2v}{dx^2} + \frac{E_a^*}{E_c^* I_c\, t_a} v = 0 \quad \text{with b.c.} \quad \begin{cases} v(L) = 0 \\ \dfrac{dv}{dx}(L) = 0 \\ V(0) = 0 \Rightarrow \dfrac{d^3v}{dx^3}(0) - \dfrac{t_c^2 G_a}{4t_a E_c^* I_c}\dfrac{dv}{dx}(0) = 0 \\ M(0) = Ne \Rightarrow \dfrac{d^2v}{dx^2}(0) = \dfrac{Ne}{E_c^* I_c} \end{cases} \tag{1}$$

where $I_c = t_c^{\,3} / 12$ is the moment of inertia and N, V and M are the compression force, the shear force and the bending moment of a unit strip of the coating. For solution convenience let us introduce two parameters α and β with dimensions of an inverse of a length

$$\alpha = \sqrt[4]{\frac{E_a^*}{4E_c^* I_c\, t_a}}, \quad \beta = \sqrt{\frac{t_c^2 G_a}{4E_c^* I_c\, t_a}} \tag{2}$$

and rewrite equation (1) in the form:

$$\frac{d^4v}{dx^4} - \beta^2 \frac{d^2v}{dx^2} + 4\alpha^4 v = 0 \tag{3}$$

By introducing the non-dimensional variables

$$s = \alpha x, \quad \ell = \alpha L, \quad w = \frac{v}{v_0}, \quad m = \frac{Ne}{\alpha^2 v_0 E_c^* I_c} \tag{4}$$

equation (3) can be more conveniently rewritten in non-dimensional form

$$\frac{d^4w}{ds^4} - \frac{\beta^2}{\alpha^2}\frac{d^2w}{ds^2} + 4w = 0 \quad \text{with b.c.} \quad \begin{cases} w(\ell) = 0 \\ \dfrac{dw}{ds}(\ell) = 0 \\ V(0) = 0 \Rightarrow \dfrac{d^3w}{ds^3}(0) - \dfrac{\beta^2}{\alpha^2}\dfrac{dw}{ds}(0) = 0 \\ M(0) = Ne \Rightarrow \dfrac{d^2w}{ds^2}(0) = m \end{cases} \tag{5}$$

The non-dimensional solution can be obtained in closed form using a symbolic manipulator

$$w(s) = m\Big[C_1 \cosh\left(\sqrt{2}\cos\vartheta\, s\right)\cos\left(\sqrt{2}\sin\vartheta\, s\right) + C_2 \cosh\left(\sqrt{2}\cos\vartheta\, s\right)\sin\left(\sqrt{2}\sin\vartheta\, s\right) + C_3 \sinh\left(\sqrt{2}\cos\vartheta\, s\right)\cos\left(\sqrt{2}\sin\vartheta\, s\right) + C_4 \sinh\left(\sqrt{2}\cos\vartheta\, s\right)\sin\left(\sqrt{2}\sin\vartheta\, s\right)\Big] \tag{6}$$

where ϑ is such that

$$\cos(2\vartheta) = \frac{1}{4}\frac{\beta^2}{\alpha^2} \tag{7}$$

and the constants C_i and Δ are given by

$$\begin{aligned} C_1 &= \frac{1}{\Delta}\Big[\cos^2\vartheta\cos\left(2\sqrt{2}\ell\sin\vartheta\right) - \sin^2\vartheta\cosh\left(2\sqrt{2}\ell\cos\vartheta\right) - \cos(2\vartheta)\Big] \\ C_2 &= \frac{1}{\Delta}\Big[\cos^2\vartheta\sin\left(2\sqrt{2}\ell\sin\vartheta\right) + \sin\vartheta\cos\vartheta\sinh\left(2\sqrt{2}\ell\cos\vartheta\right)\Big] \\ C_3 &= \frac{1}{\Delta}\Big[\cos\vartheta\sin\vartheta\sin\left(2\sqrt{2}\ell\sin\vartheta\right) + \sin^2\vartheta\sinh\left(2\sqrt{2}\ell\cos\vartheta\right)\Big] \\ C_4 &= -\frac{1}{\Delta}\Big[\cos\vartheta\sin\vartheta\cos\left(2\sqrt{2}\ell\sin\vartheta\right) + \cos\vartheta\sin\vartheta\cosh\left(2\sqrt{2}\ell\cos\vartheta\right) + \sin(2\vartheta)\Big] \\ \Delta &= \Big[\cos(4\vartheta) - \cos(2\vartheta)\Big]\cosh\left(2\sqrt{2}\ell\cos\vartheta\right) + \Big[\cos(4\vartheta) + \cos(2\vartheta)\Big]\cos\left(2\sqrt{2}\ell\sin\vartheta\right) - 2 \end{aligned} \tag{8}$$

The critical bending moment m corresponding to the attainment of the limit elastic displacement v_0 at $s = 0$ is obtained by setting $w(0) = 1$ in (6), which gives

$$m = \frac{1}{C_1} \tag{9}$$

and hence

$$N_P^{cr.el.}(0) = \frac{\alpha^2 v_0 E_c^* I_c}{eC_1} \tag{10}$$

The Winkler type solution corresponding to $k_2 = 0$ can be obtained from (6) by simply setting $\beta = 0$ and reads (subscript W stands for Winkler-type solution)

$$N_W^{cr.el.} = \frac{v_0}{e}\sqrt{\frac{E_a^* E_c^* I_c}{t_a}} \tag{11}$$

In the following developments, reference will be made to the specific geometry and material properties reported in Table 1, representative of a typical engineering tile cladding configuration, where the coating is composed by a sequence of tiles and the substrate is a concrete layer. With these values, the transverse displacement $w = v / v_0$ in (6), for assigned bending moment $M(0) = N_W^{cr.el.} e$, where $N_W^{cr.el.}$ is given in (11), is plotted in Figure 4 for different values of the parameter β.

Table 1 – Parameter definition for considered model problem

$t_c = 8$ mm	$E_c = 50$ GPa	$\nu_c = 0.2$
$t_a = 3$ mm	$E_a = 3.5$ GPa	$\nu_a = 0.3$
$t_s = 40$ mm	$E_s = 22$ GPa	$\nu_s = 0.175$
$v_0 = 1.87 \times 10^{-3}$ mm	$\sigma_0 = 2.4$ MPa	$L = 400$ mm
$\alpha = 0.1096$ mm^{-1}	$\alpha L = 43.84$	$e = t_c / 2 = 4$ mm
$\beta = 0.05684$ mm^{-1}	$\beta L = 22.74$	$\vartheta = 0.75$
$\zeta = 0.063$ mm^{-1}	$\zeta L = 25.44$	$\hat{\vartheta} = 0.19$
$\bar{v} = 0.066$ mm	$\tau_0 = 2.4$ MPa	$G_f = 0.08$ N/mm

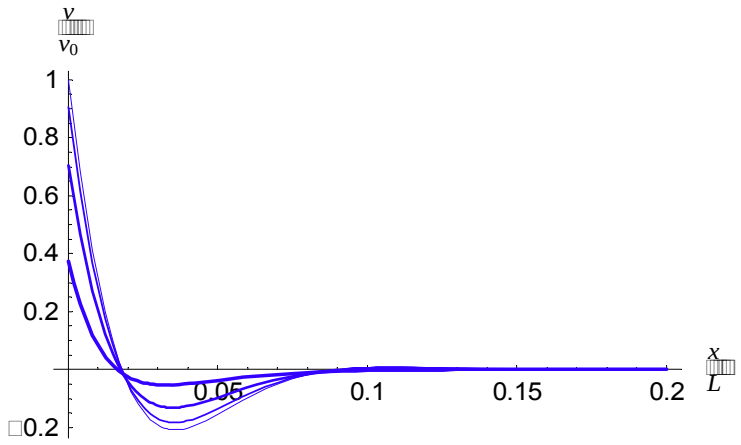

Figure 4 – Deflection of the tile for different βL; $\beta L = 0$ (finer curve), 0.05, 0.1 and 0.2 (thicker curve).

When considering the shear stiffness of the adhesive, there are shear stresses on the tile bottom surface and, for equilibrium reasons, the resulting axial forces varies along the tile. Hence $N_P^{cr.el.}$ varies along the tile length. The resultant F_τ of these shear stresses can be computed from the Pasternak solution (6) as

$$F_\tau = \int_0^L -\frac{G_a t_c}{2t_a}\frac{dv}{dx}dx = \frac{G_a t_c}{2t_a}v(0) \tag{12}$$

The value in correspondence of the attainment of the critical opening $v(0) = v_0$, does not require the solution of (3) and is simply

$$F_\tau^{cr.el.} = \frac{G_a\, t_c}{2t_a}v_0 \tag{13}$$

Outside the debonding zone, the tile deflection tends to vanish together with the shear stresses in the adhesive. As a consequence, the axial force remains constant. The critical axial force $N_P^{cr.el.}(L)$ at the end of the tile is obtained from the tile horizontal equilibrium (see Figure 5) as

$$N_P^{cr.el.}(L) = N_P^{cr.el.}(0) + F_\tau^{cr} \tag{14}$$

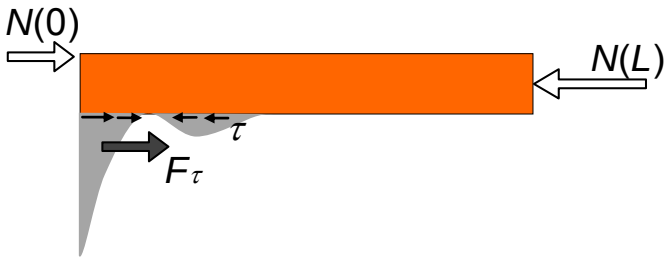

Figure 5 – Free body diagram of the tile including shear stresses (only horizontal forces are shown).

It is remarkable that, for a wide range of parameters including the values listed in Table 1, numerically one has $F_\tau^{cr} \approx \frac{2e}{t_c}\left(N_P^{cr.el.}(0) - N_W^{cr.el.}\right)$. Figure 6 shows the ratio $N_P^{cr.el.}(0)/(N_W^{cr.el.} + \frac{t_c}{2e}F_\tau^{cr})$ for $e = t_c/2$, as a function of α, for different values of tile length L. From this parametric study it appears that the ratio is ≈ 1 whenever $\alpha L > 5$, condition which is satisfied for the range of material and geometric parameters of usual tile flooring. One can therefore obtain a simple estimate of the tile compressive force at the decohesion elastic limit $N_P^{cr.el.}(L)$, outside the debonding zone, which accounts for the shear stiffness of the adhesive

$$N_P^{cr.el.}(L) = N_W^{cr.el.} + \left(1 + \frac{t_c}{2e}\right)F_\tau^{cr.el.} = \frac{v_0}{e}\sqrt{\frac{E_a^* E_c^* I_c}{t_a}} + \left(1 + \frac{t_c}{2e}\right)\frac{G_a\, t_c}{2t_a}v_0 \tag{15}$$

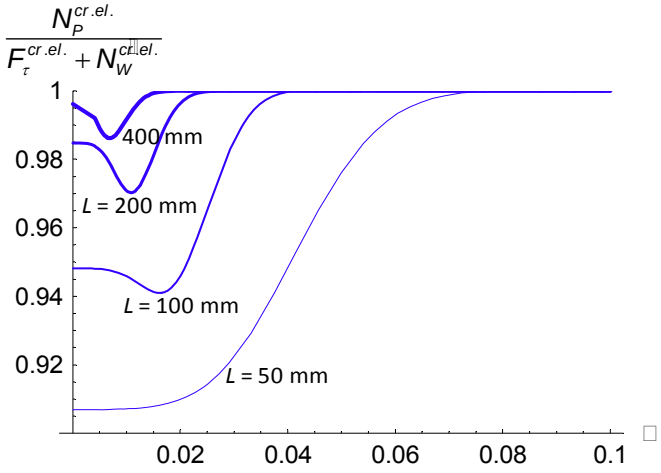

Figure 6 – Ratio between the exact Pasternak solution and the approximate solution given in Eq. (15).

3 COHESIVE CRACK DEBONDING LIMIT

The ultimate strength of the coating is obtained assuming that a cohesive process zone of length L_{pz} can develop along the adhesive interface. The rigid-cohesive behavior shown in Figure 3b is assumed for the normal stress, while the shear behaviour is assumed to remain elastic. In this case the coating transverse displacement is governed by the following differential equation

$$\frac{d^4v}{dx^4} - \frac{t_c^2 G_a}{4 t_a E_c^* I_c}\frac{d^2v}{dx^2} - \frac{\sigma_0}{E_c^* I_c \bar{v}} v = -\frac{\sigma_0}{E_c^* I_c} \quad \text{with b.c.} \quad \begin{cases} v(L_{pz}) = 0 \\ \dfrac{dv}{dx}(L_{pz}) = 0 \\ V(0) = 0 \Rightarrow \dfrac{d^3v}{dx^3}(0) - \dfrac{t_c^2 G_a}{4 t_a E_c^* I_c}\dfrac{dv}{dx}(0) = 0 \\ M(0) = Ne \Rightarrow \dfrac{d^2v}{dx^2}(0) = \dfrac{Ne}{E_c^* I_c} \end{cases} \tag{16}$$

The condition $dv/dx(L_{pz}) = 0$ accounts for the fact that no singularity exists at the tip of the cohesive process zone.

Using the definition of β given in Eq. $(2)_2$, introducing another parameter ζ with the dimensions of the inverse of a length

$$\zeta = \sqrt[4]{\frac{\sigma_0}{E_c^* I_c \bar{v}}} \tag{17}$$

where $\bar{v}$ is the limit opening displacement of the cohesive model (Figure 3b), and introducing the following non-dimensional quantities

$$\hat{w} = \frac{v}{\bar{v}}, \quad \hat{s} = \zeta x, \quad \hat{\ell} = \zeta L_{pz}, \quad \hat{m} = \frac{Ne}{\bar{v}\zeta^2 E_c^* I_c} \tag{18}$$

also in this case the problem can be conveniently formulated in non-dimensional form:

$$\frac{d^4\hat{w}}{d\hat{s}^4}-\frac{\beta^2}{\zeta^2}\frac{d^2\hat{w}}{d\hat{s}^2}-\hat{w}=-1 \quad \text{with b.c.} \quad \begin{cases} \hat{w}\left(\hat{\ell}\right)=0 \\ \dfrac{d\hat{w}}{d\hat{s}}\left(\hat{\ell}\right)=0 \\ V(0)=0\Rightarrow \dfrac{d^3\hat{w}}{d\hat{s}^3}(0)-\dfrac{\beta^2}{\zeta^2}\dfrac{d\hat{w}}{d\hat{s}}(0)=0 \\ M(0)=Ne\Rightarrow \dfrac{d^2\hat{w}}{d\hat{s}^2}(0)=\hat{m} \end{cases} \tag{19}$$

After integration of the differential equation and enforcement of the boundary conditions, the transversal displacement in non-dimensional form is given by

$$\hat{w}\left(\hat{s}\right)=1+\hat{C}_1\cosh\left(e^{\hat{\vartheta}}\hat{s}\right)+\hat{C}_2\sinh\left(e^{\hat{\vartheta}}\hat{s}\right)+\hat{C}_3\cos\left(e^{-\hat{\vartheta}}\hat{s}\right)+\hat{C}_4\sin\left(e^{-\hat{\vartheta}}\hat{s}\right) \tag{20}$$

where the non-dimensional parameter $\hat{\vartheta}$ is defined by

$$\sinh\left(2\hat{\vartheta}\right)=1/2\left(\beta/\zeta\right)^2 \tag{21}$$

and the constants $\hat{C}_i$ and $\hat{\Delta}$ are defined as

$$\hat{C}_1=\frac{1}{\hat{\Delta}}\left\{-\hat{m}\left[e^{-2\hat{\vartheta}}+e^{2\hat{\vartheta}}\cosh\left(\hat{\ell}e^{\hat{\vartheta}}\right)\cos\left(\hat{\ell}e^{-\hat{\vartheta}}\right)+\sinh\left(\hat{\ell}e^{\hat{\vartheta}}\right)\sin\left(\hat{\ell}e^{-\hat{\vartheta}}\right)\right]+\left[\cosh\left(\hat{\ell}e^{\hat{\vartheta}}\right)+e^{-4\hat{\vartheta}}\cos\left(\hat{\ell}e^{-\hat{\vartheta}}\right)\right]\right\}$$

$$\hat{C}_2=\frac{1}{\hat{\Delta}}\left\{\hat{m}\left[e^{2\hat{\vartheta}}\sinh\left(\hat{\ell}e^{\hat{\vartheta}}\right)\cos\left(\hat{\ell}e^{-\hat{\vartheta}}\right)+\cosh\left(\hat{\ell}e^{\hat{\vartheta}}\right)\sin\left(\hat{\ell}e^{-\hat{\vartheta}}\right)\right]+\left[-\sinh\left(\hat{\ell}e^{\hat{\vartheta}}\right)+e^{2\hat{\vartheta}}\sin\left(\hat{\ell}e^{-\hat{\vartheta}}\right)\right]\right\}$$

$$\hat{C}_3=\frac{1}{\hat{\Delta}}\left\{\hat{m}\left[e^{2\hat{\vartheta}}+e^{-2\hat{\vartheta}}\cosh\left(\hat{\ell}e^{\hat{\vartheta}}\right)\cos\left(\ell e^{-\hat{\vartheta}}\right)-\sinh\left(\hat{\ell}e^{\hat{\vartheta}}\right)\sin\left(\ell e^{-\hat{\vartheta}}\right)\right]+\left[e^{4\hat{\vartheta}}\cosh\left(\hat{\ell}e^{\hat{\vartheta}}\right)+\cos\left(\hat{\ell}e^{-\hat{\vartheta}}\right)\right]\right\}$$

$$\hat{C}_4=\frac{1}{\hat{\Delta}}\left\{\hat{m}\left[e^{-2\hat{\vartheta}}\cosh\left(\ell e^{\hat{\vartheta}}\right)\sin\left(\hat{\ell}e^{-\hat{\vartheta}}\right)+\sinh\left(\ell e^{\hat{\vartheta}}\right)\cos\left(\hat{\ell}e^{-\hat{\vartheta}}\right)\right]+\left[-e^{-2\hat{\vartheta}}\sinh\left(\hat{\ell}e^{\hat{\vartheta}}\right)+\sin\left(\hat{\ell}e^{-\hat{\vartheta}}\right)\right]\right\}$$

$$\hat{\Delta}=-2\left[1+\cosh\left(4\hat{\vartheta}\right)\cosh\left(\hat{\ell}e^{\hat{\vartheta}}\right)\cos\left(\hat{\ell}e^{-\hat{\vartheta}}\right)+\sinh\left(2\hat{\vartheta}\right)\sinh\left(\hat{\ell}e^{\hat{\vartheta}}\right)\sin\left(\hat{\ell}e^{-\hat{\vartheta}}\right)\right] \tag{22}$$

The length L_{pz} of the process zone can be computed by imposing $v(0)=\bar{v}$ or, in non-dimensional form, $w(0)=1$, i.e.:

$$\hat{w}(0)=1+\frac{2\hat{m}\left[-\sinh\left(2\hat{\vartheta}\right)+\sinh\left(\hat{\ell}e^{\hat{\vartheta}}\right)\sin\left(\hat{\ell}e^{-\hat{\vartheta}}\right)+\sinh\left(2\hat{\vartheta}\right)\cosh\left(\hat{\ell}e^{\hat{\vartheta}}\right)\cos\left(\hat{\ell}e^{-\hat{\vartheta}}\right)\right]}{2\left[1+\cosh\left(4\hat{\vartheta}\right)\cosh\left(\hat{\ell}e^{\hat{\vartheta}}\right)\cos\left(\hat{\ell}e^{-\hat{\vartheta}}\right)+\sinh\left(2\hat{\vartheta}\right)\sinh\left(\hat{\ell}e^{\hat{\vartheta}}\right)\sin\left(\hat{\ell}e^{-\hat{\vartheta}}\right)\right]}-$$

$$\frac{\left[\left(1+e^{-4\vartheta}\right)\cos\left(\hat{\ell}e^{-\vartheta}\right)+\left(1+e^{4\vartheta}\right)\cosh\left(\hat{\ell}e^{\vartheta}\right)\right]}{2\left[1+\cosh\left(4\hat{\vartheta}\right)\cosh\left(\hat{\ell}e^{\hat{\vartheta}}\right)\cos\left(\hat{\ell}e^{-\hat{\vartheta}}\right)+\sinh\left(2\hat{\vartheta}\right)\sinh\left(\hat{\ell}e^{\hat{\vartheta}}\right)\sin\left(\hat{\ell}e^{-\hat{\vartheta}}\right)\right]}=1 \tag{23}$$

Solving this equation for $\hat{m}$ provides the following expression which depends on the non-dimensional length $\hat{\ell}$ of the process zone

$$\hat{m}\left(\hat{\ell}\right)=\frac{1}{2}\left[\frac{\left(1+e^{-4\hat{\vartheta}}\right)\cos\left(\hat{\ell}e^{-\hat{\vartheta}}\right)+\left(1+e^{4\hat{\vartheta}}\right)\cosh\left(\hat{\ell}e^{\vartheta}\right)}{-\sinh\left(2\hat{\vartheta}\right)+\sinh\left(\hat{\ell}e^{\hat{\vartheta}}\right)\sin\left(\hat{\ell}e^{-\hat{\vartheta}}\right)+\sinh\left(2\hat{\vartheta}\right)\cosh\left(\hat{\ell}e^{\hat{\vartheta}}\right)\cos\left(\hat{\ell}e^{-\hat{\vartheta}}\right)}\right] \tag{24}$$

The critical condition is assumed to be attained for the minimum value of $\hat{m}\left(\hat{\ell}\right)$ for which the ultimate separation $\bar{v}$ is reached at $x = 0$. This turns out to be given by:

$$\frac{d\hat{m}\left(\hat{\ell}\right)}{d\hat{\ell}} = 0 \tag{25}$$

Equation (25) implicitly defines the critical length of the process zone $\hat{\ell}_{cr}$, which is a function of the material parameters and geometry through $\hat{\vartheta}$ defined in Eq. (21). The critical value $\hat{m}_{cr} = \hat{m}\left(\hat{\ell}_{cr}\right)$ of the moment at decohesion can then be obtained from (24) by setting $\hat{\ell} = \hat{\ell}_{cr}$. Even though $\hat{\ell}_{cr}$ cannot be given an explicit expression, it can be numerically computed from (25) for assigned $\hat{\vartheta}$ and then substituted in Eqs. (24) and (20) to obtain the solution at decohesion in terms of critical bending moment and coating displacement. From Table 1, for the considered reference problem one has $\hat{\vartheta} = 0.19$ which, from (25), gives $\hat{\ell}_{cr} = 1.79$. If instead $\hat{\vartheta} = 0$, corresponding to vanishing shear stiffness in the adhesive, is used one obtains $\hat{\ell}_{cr} = 1.87$, with an error on $\hat{\ell}_{cr}$ of 1.1%.

The influence of the adhesive shear stiffness on the solution is further evidenced in Figures 7a and 7b. Figure 7 shows the vertical tile displacement along the process zone obtained with the adhesive shear stiffnesses $G_a = 0$ MPa, 673 MPa, 1346 MPa, which correspond to $\hat{\vartheta} = 0$, $\hat{\vartheta} = 0.10$, $\hat{\vartheta} = 0.19$, a very similar distribution is obtained. Since the normal tractions $\sigma(x)$ in the tile-adhesive interface are proportional to the displacement as in Figure 3, one can conclude that the normal traction distribution obtained neglecting the shear stiffness ($\hat{\vartheta} = 0$) is a reasonable approximation, in particular in the case of tile floorings of practical interest.

Unlike for the displacements, the shear stiffness greatly affects the distribution of the tangential stresses between the tile and the adhesive as shown in Figure 7b. The value of shear stresses corresponding to the material parameters of Table 1 ($G_a = 1346$ MPa) are very large and certainly not compatible for a real adhesive with the assumed purely elastic shear behavior. The correct solution of the problem would require the formulation, on the basis of experimental results, of a proper mixed mode decohesion model for the adhesive. However, the above analysis shows that both the length of the critical process zone and the normal stress distribution are almost independent of the assumed shear behavior of the adhesive. This conclusion can be used to obtain an estimate of the maximum compression force sustainable by the tiles without causing decohesion from the adhesive.

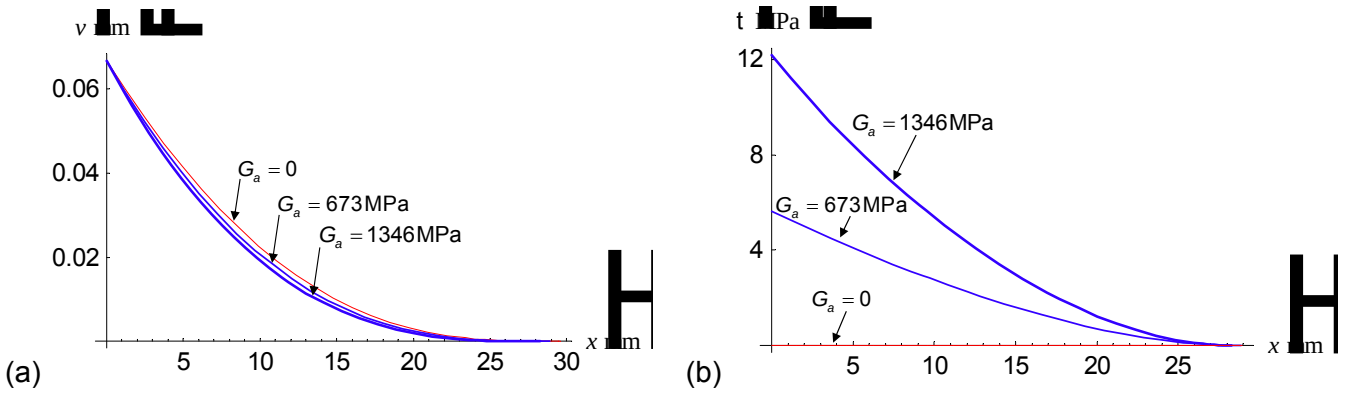

Figure 7 – (a) Vertical tile displacement for different adhesive shear stiffness. (b) Tangential stress for varying adhesive shear stiffness.

To the purpose of assessing the critical value of the coating compression leading to coating decohesion, consider the free body diagram of the coating at the decohesion limit ($\hat{w}(0)=1$), either neglecting or considering shear stresses (Figure 8). The quantities related to the case without shear stresses in the left sketch are labeled with subscript W (Winkler-type model). Hence, denoting by σ_W the normal tractions between tile and adhesive in the Winkler case, global equilibrium for the two cases reads (see Figure 8 for a pictorial interpretation of symbols):

$$N_W(0)=N_W\left(L_{pz_W}\right);\qquad N_W(0)e=\int_0^{L_{pz_W}}\sigma_W\left(L_{pz_W}-x\right)dx$$

$$N(0)+F_\tau=N\left(L_{pz}\right);\qquad N(0)e=F_\tau\frac{t_t}{2}+\int_0^{L_{pz}}\sigma\left(L_{pz}-x\right)dx \tag{26}$$

As discussed in the previous section, from the comparison of the deflected shapes in Figure 7a, one can assume $L_{pz}\approx L_{pz_W}$ and $\sigma\approx\sigma_W$ obtaining from (26)

$$N\left(L_{pz}\right)\approx N_W(0)+F_\tau\left(1+\frac{t_t}{2e}\right) \tag{27}$$

This result extends to the nonlinear case the relation (15) obtained for the elastic solution and allows to compute an estimate of the critical compression force in the coating at the decohesion limit $N^{cr.coh.}$, provided that the critical compression force in the limit of zero shear stiffness $N_W^{cr.coh.}$ and the critical resultant of the shear stresses $F_\tau^{cr.coh.}$ at the decohesion limit are known

$$N^{cr.coh.}\approx N_W^{cr.coh.}+F_\tau^{cr.coh.}\left(1+\frac{t_t}{2e}\right) \tag{28}$$

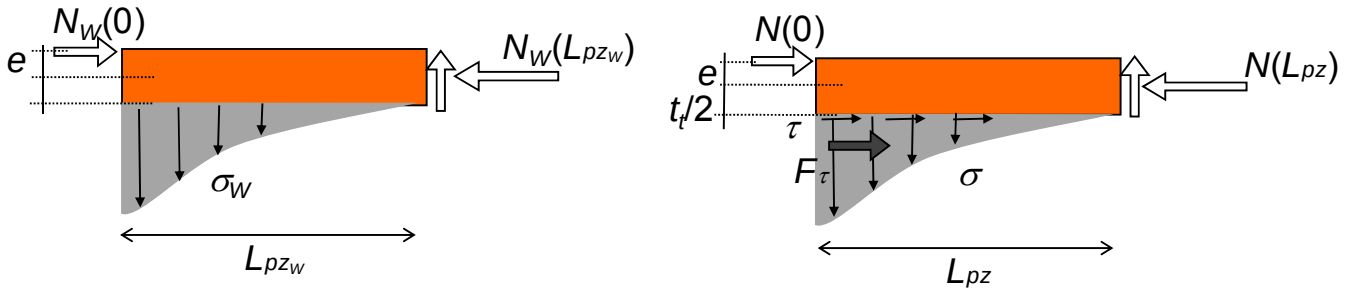

Figure 8 – Coating free body diagram neglecting shear stresses (left sketch, index W) and considering shear stresses (rigth sketch).

The value of $N_W^{cr.coh.}$ can be obtained as a special case from the above analysis setting $\beta=0$ and hence $\hat{\vartheta}=0$. In this case, the solution greatly simplifies and one can find closed form expressions to be used in the simplified analysis of debonding. In particular, Eq. (24) simplifies to

$$\hat{m}\left(\hat{\ell}\right)\Big|_{\hat{\vartheta}=0}=\frac{\cos\hat{\ell}+\cosh\hat{\ell}}{\sinh\hat{\ell}\sin\hat{\ell}} \tag{29}$$

and the critical condition reads

$$\frac{d\hat{m}}{d\hat{\ell}}=0\Rightarrow\cos\hat{\ell}_{cr}\cosh\hat{\ell}_{cr}+1=0 \tag{30}$$

from which the following non-dimensional values of the process zone length and of the moment are found

$$\hat{\ell}_{cr} = 1.8751; \qquad \hat{m}_{cr}\big|_{\hat{\vartheta}=0} = 1 \tag{31}$$

Note that the last equality follows from Eqs. (29) and (30) using the identity:

$$\sinh \hat{\ell}_{cr} \sin \hat{\ell}_{cr} = \sqrt{\cosh^2 \hat{\ell}_{cr} - 1}\sqrt{1 - \cos^2 \hat{\ell}_{cr}}$$

Imposing $\hat{m}_{cr}\big|_{\hat{\vartheta}=0} = 1$, from (17) and $(18)_4$, one can obtain the critical coating compression leading to decohesion

$$N_W^{cr.coh.} = \frac{\bar{v}}{e}\sqrt{\frac{\sigma_0 E_t^* I_t}{\bar{v}}} \tag{32}$$

The value of $F_\tau^{cr.coh.}$ in (27) cannot be deduced from the solution of Eq. (16) since, as already remarked, the values of τ computed in that way would exceed the shear strength of the adhesive. A first, simple estimate of $F_\tau^{cr.coh.}$ can be obtained assuming a linear distribution of τ in the process zone with maximum value equal to the shear strength of the adhesive τ_0.

$$F_\tau^{cr.coh.} \approx \frac{1}{2}\frac{\hat{\ell}_{cr}}{\zeta}\tau_0 = \frac{1.8751}{2}\sqrt[4]{\frac{E_t^* I_t \bar{v}}{\sigma_0}}\tau_0 \tag{33}$$

Using (32) and (33) in Eq. (28) one obtains

$$N^{cr.coh.} \approx \frac{\bar{v}}{e}\sqrt{\frac{\sigma_0 E_t^* I_t}{\bar{v}}} + \frac{1.8751}{2}\sqrt[4]{\frac{E_t^* I_t \bar{v}}{\sigma_0}}\tau_0\left(1 + \frac{t_t}{2e}\right) \tag{34}$$

which gives a simple closed form expression to evaluate the cohesisve crack debonding limit of the coating.

4 CONCLUSIONS

A simplified approach has been proposed for the estimation of the ultimate strength of a coating-substrate adhesive joint under a compression force applied to the coating with a known eccentricity. This problem can be representative of the one occuring in civil tile claddings, under assigned temperature variation and/or other sources of inelastic substrate shrinking. The proposed approach leads to simple closed formulas which require the knowledge of a limited number of parameters. The procedure can be easily implemented in a spreadsheet and used for the selection of the most appropriate adhesive for a given joint configuration.

5 REFERENCES

ANDRUET, R. H.; DILLARD, D. A.; HOLZER, S. M. Two- and three-dimensional geometrical nonlinear finite elements for analysis of adhesive joints. **International Journal of Adhesion and Adhesives**, v. 21, n.1, p.17-34, 2001.

BIGWOOD, D.; CROCOMBE, A. **Elastic analysis and engineering design formulae for bonded joints,** International Journal of Adhesion and Adhesives, v. 9, n. 4, p. 229-242, 1989.

CARPINTERI, A.; PAGGI, M.; ZAVARISE, G. The effect of contact on the decohesion of laminated beams with multiple microcracks. **International Journal of Solids and Structures**, v. 45, n. 1, p.129-143, 2008.

DE LORENZIS, L.; ZAVARISE, G. Modeling of mixed-mode debonding in the peel test applied to

superficial reinforcements. **International Journal of Solids and Structures**, v. 45, n. 20, p. 5419-5436, 2008.

EDLUND, U.; SCHMIDT, P.; ROGUET, E. A model of an adhesively bonded joint with elastic-plastic adherends and a softening adhesive. **Computer Methods in Applied Mechanics and Engineering**, v. 198, n. 5-8, p. 740-752, 2009.

FERREIRA, M. D. C.; VENTURINI, W. S.; HILD, F., On the analysis of notched concrete beams: From measurement with digital image correlation to identification with boundary element method of a cohesive model. **Engineering Fracture Mechanics**, n. 78, v. 1, p. 71-84, 2011.

GOLAND, M.; REISSNER, E. The stresses in cemented joints. **Journal of Applied Mechanics**, 11:A–17; A–27, 1944.

GONÇALVES, J. P. M.; DE MOURA, M. F. S. F.; DE CASTRO, P. M. S. T. A three-dimensional finite element model for stress analysis of adhesive joints. **International Journal of Adhesion & Adhesives**, n. 22, p. 357-365, 2002.

GUSTAFSON, P. A.; WAAS, A. M. The influence of adhesive constitutive parameters in cohesive zone finite element models of adhesively bonded joints. **International Journal of Solids and Structures**, v. 46, n. 10, p. 2201-2215, 2009.

LEONEL, E. D.; VENTURINI, W. S., Non-linear boundary element formulation with tangent operator to analyse crack propagation in quasi-brittle materials, **Engineering Analysis with Boundary Elements**, v. 34, n. 2, p. 122-129, 2010.

LEONEL, E .D.; VENTURINI, W. S. Cohesive crack propagation using a boundary element formulation with a tangent operator, **WIT Transactions on Modelling and Simulation**, n. 49, p. 247-255, 2009.

MAHABOONPACHAI, T.; MATSUMOTO, T.; INABA, Y. Investigation of interfacial fracture toughness between concrete and adhesive mortar in an external wall tile structure. **International Journal of Adhesion and Adhesives**, v. 30, n. 1, p. 1–9, 2010.

MANZOLI, O. L.; VENTURINI, W. S. An implicit BEM formulation to model strong discontinuities in solids, **Computational Mechanics**, v. 40, n. 6, p. 901-909, 2007.

PASTERNAK, P. Fundamentals of a new method of analysis of structures on elastic foundation by means of two subgrade coefficients (in Russian). **Gosudarstvennoe Izdatel'stvo Literatury po Stroitel'stvu I Arkhitekture**, 1954.

SCHMIDT, P.; EDLUND, U. Analysis of adhesively bonded joints: a finite element method and a material model with damage. **International Journal for Numerical Methods in Engineering**, v. 66, n. 8, p.1271-1308, 2006.

THOULESS, M. D.; JENSEN, H. M. Elastic fracture mechanics of the peel-test geometry. **The Journal of Adhesion**, v. 38, n. 3, p. 185-197, 1992.

YUAN, H.; CHEN, J.; TENG, J.; LU, X. Interfacial stress analysis of a thin plate bonded to a rigid substrate and subjected to inclined loading. **International Journal of Solids and Structures**, v. 44, n. 16, p. 5247-5271, 2007.

TONG, L. Strength of adhesively bonded single-lap and lap-shear joints. **International Journal of Solids and Structures**, v. 35, n. 20, p. 2601-2616, 1998.

TSAI, M. Y.; OPLINGER, D. W.; MORTON, J. Improved theoretical solutions for adhesive lap joints. **International Journal of Solids and Structures**, v., 35, n. 12, p. 1163-1185, 1998.

VOLKERSEN, O. The elasticity and strength of paper and other fibrous materials. **Luftfahrtforschung**, n. 15, p. 41-47, 1938.

YANG, C.; HUANG, H.; TOMBLIN, J. S.; SUN, W. Elastic-plastic model of adhesive-bonded single-lap composite joints. **Journal of Composite Materials**, v. 38, n. 4, p. 293-309, 2004.

WILLIAMS, J. G., Energy Release Rates for the Peeling of Flexible Membranes and the Analysis of Blister Tests. **International Journal of Fracture**, v.87, n. 3, p. 265-288, 1997.

WILLIAMS, J.; HADAVINIA, H. Analytical solutions for cohesive zone models. **Journal of the Mechanics and Physics of Solids**, v. 50, n. 4, p.809-825, 2002.